

Hybrid Receiver Design for Massive MIMO-OFDM with Low-Resolution ADCs and Oversampling

Mengyuan Ma, Nhan Thanh Nguyen, Italo Atzeni, and Markku Juntti
Centre for Wireless Communications (CWC), University of Oulu, Finland
E-mail: {mengyuan.ma, nhan.nguyen, italo.atzeni, markku.juntti}@oulu.fi

Abstract—Low-resolution analog-to-digital converters (ADCs) and hybrid beamforming have emerged as efficient solutions to reduce power consumption with satisfactory spectral efficiency (SE) in massive multiple-input multiple-output (MIMO) systems. In this paper, we investigate the performance of a hybrid receiver in uplink massive MIMO orthogonal frequency-division multiplexing (OFDM) systems with low-resolution ADCs and oversampling. Considering both the temporal and spatial correlation of the quantization distortion (QD), we derive a closed-form approximation of the frequency-domain QD covariance matrix, which facilitates the evaluation of the system SE. Then we jointly design the analog and baseband combiners to maximize the SE. The formulated problem is significantly challenging due to the constant-modulus constraint of the analog combiner and its coupling with the digital one. To overcome the challenges, we transform the objective function into an equivalent but more tractable form and then iteratively update the analog and digital combiner. Numerical simulations verify the superiority of the proposed algorithm compared to the considered benchmarks and show the resilience of the hybrid receiver to beam squint for low-resolution systems. Furthermore, the results show that the proposed hybrid receiver design with oversampling can achieve significantly higher energy efficiency compared to the digital one.

Index Terms—Massive MIMO-OFDM, energy efficiency, low-resolution ADCs, oversampling, hybrid receiver.

I. INTRODUCTION

Massive multiple-input multiple-output (MIMO) technology stands as a pivotal cornerstone in the advancement of future wireless systems [1], leveraging its vast array of antennas at the base station (BS) to deliver exceptional spectral efficiency (SE) [2]. However, the deployment of massive MIMO at millimeter wave and (sub-)THz frequencies introduces a significant challenge: the substantial power consumption of numerous radio-frequency (RF) chains threatens to undermine its energy efficiency (EE) [3], [4]. Among RF components, analog-to-digital converters (ADCs) are the most power-hungry parts, as their power consumption increases exponentially with the number of resolution bits [5]. For instance, 8–12-bit high-speed ADCs operating at 1 Gsample/s can consume several Watts [6], which motivates the application of low-resolution ADCs. On the other hand, hybrid

beamforming technique can effectively reduce the required number of RF chains without unduly compromising SE [7]. In this context, the integration of low-resolution ADCs within hybrid beamforming architectures emerges as a compelling strategy to balance energy cost and SE performance [8], [9].

The performance of a hybrid receiver with low-resolution ADCs was investigated [9]–[11], demonstrating a flexible tradeoff between power consumption and SE performance. However, these works mainly focus on narrowband single-carrier systems, and thus, their results may not be valid for wideband multi-carrier (sub-)THz communications systems. This is because the frequency-flat analog beamformer must be designed for all subcarriers, and the correlation of time-domain symbols after quantization significantly involves frequency-domain performance analysis [12]. The uplink performance of wideband MIMO orthogonal-frequency-division-multiplexing (OFDM) with low-resolution ADCs was investigated in [13]–[16]. It was shown in [13], [14] that few-bit quantization in MIMO-OFDM systems can approach the performance of the infinite-precision case. Ma *et al.* [16] studied the performance of oversampling in an MIMO-OFDM uplink, showing that oversampling can significantly enhance the sum rate, especially at high signal-to-noise ratios (SNRs) and with very low ADC resolutions. However, fully digital receivers were considered in [13]–[16], which have limited applications in high-frequency massive MIMO systems because of the requirement of an excessively large number of RF chains.

Unlike most of the aforementioned works, we herein investigate an uplink high-frequency massive MIMO-OFDM system employing both hybrid beamformer and low-resolution ADCs. Specifically, we first derive a closed-form approximation for the frequency-domain covariance matrix of the quantization distortion based on the Busgang decomposition, which considers the temporal and spatial correlation of the quantization distortion. With the facilitation of the approximation, we jointly design the analog and baseband combiners to maximize the SE. The formulated problem is significantly challenging due to the constant-modulus constraint of the analog combiner and its coupling with the digital one. To overcome the challenges, we transform the objective function into an equivalent but more tractable form and then iteratively update the analog and digital combiner. Numerical simulations verify the superiority of the proposed algorithm compared to

This work was supported by the Academy of Finland (332362 EERA, 336449 Profi6, 346208 6G Flagship, 348396 HIGH-6G, and 357504 EET-CAMD), Infotech Oulu, and the European Commission (101095759 Hexa-X-II).

the benchmarks considered. Furthermore, the results show that the performance degradation of the hybrid receiver due to the notorious beam squint effect [17], [18] is less significant for low-resolution systems. Additionally, the EE comparison shows that the proposed hybrid receiver design with oversampling significantly outperforms the considered digital receiver.

II. SYSTEM MODEL

A. Signal Model

We consider an uplink massive MIMO system where a BS equipped with N_r antennas receives signals from the I single-antenna user equipments (UEs). We assume that the BS deploys the fully connected hybrid beamforming architecture in which each RF chain connects to all antennas through a phase-shifter network. Let N_{RF} be the number of RF chains at the BS. The OFDM is assumed over a wideband channel to deal with the frequency selectivity. Specifically, let $\Delta f = \frac{1}{T_u}$ be the subcarrier spacing, where T_u denotes the OFDM symbol duration, which is assumed to be fixed. Let $f_k = f_c + (k + 1 - \frac{N_c + 1}{2})\Delta f$, $k = 0, \dots, N_c - 1$, denote the k -th subcarrier frequency, where f_c is the center carrier frequency. Among the total N_c subcarriers, K subcarriers are employed for signal transmission, while other $N_c - K$ subcarriers are employed for oversampling [12]. Let $\tilde{s}_i[k]$ be the transmit symbol of the i -th UE at subcarrier k with $\mathbb{E}[\tilde{s}_i[k]^2] = 1$, $k = 0, \dots, K - 1$. Note that $\tilde{s}_i[k] = 0$ for $k = K, \dots, N_c - 1$ when $N_c > K$. Because the sampling frequency is $f_s = N_c \Delta f$ while the transmission bandwidth of signals is $B_w = K \Delta f$, the oversampling ratio (OSR) is defined as $\beta = \frac{N_c}{K}$. Hence, $\beta = 1$ and $\beta > 1$ indicate the Nyquist sampling and the oversampling scheme, respectively. The time-domain symbol is obtained by N_c -points inverse discrete Fourier transform, which can be expressed as

$$s_i[n] = \frac{\sqrt{p}}{\sqrt{N_c}} \sum_{k=0}^{N_c-1} \tilde{s}_i[k] e^{j \frac{2\pi n k}{N_c}}, \quad n = 0, \dots, N_c - 1, \quad (1)$$

where n represents the index of the time-domain symbol, and p denotes the average transmit power. At the receiver, the time-domain signals are first downconverted to the baseband and transformed back to the frequency domain by N_c -points discrete Fourier transform (DFT).

Let $\mathbf{s}[n] = [s_1[n], \dots, s_I[n]]^T$. The discrete-time received signal at time sample n at the BS is given by

$$\mathbf{r}[n] = \sum_{d=0}^{D-1} \mathbf{H}[d] \mathbf{s}[n-d] + \mathbf{w}[n], \quad (2)$$

where $D = \beta D_0$ with D_0 being the maximum number of delay taps under Nyquist sampling, and $\mathbf{H}[d] = [\mathbf{h}_1[d], \dots, \mathbf{h}_I[d]] \in \mathbb{C}^{N_r \times I}$ denotes the channel matrix at the d -th time delay with $\mathbf{h}_i[d]$ representing the channel between the i -th UE and the BS. Here, $\mathbf{w}[n]$ represents the additive white Gaussian noise (AWGN) vector following the distribution $\mathcal{CN}(\mathbf{0}, \sigma_n^2 \mathbf{I})$, where σ_n^2 denotes the noise variance. By taking the DFT of both sides of (2), the frequency-domain received signal is expressed as

$$\tilde{\mathbf{r}}[k] = \sqrt{p} \tilde{\mathbf{H}}[k] \tilde{\mathbf{s}}[k] + \tilde{\mathbf{w}}[k], \quad k = 0, \dots, N_c - 1, \quad (3)$$

where $\tilde{\mathbf{s}}[k] = [\tilde{s}_1[k], \dots, \tilde{s}_I[k]]^T$, with $\tilde{s}_i[k]$ being the frequency-domain signal transmitted by the i -th UE, $\tilde{\mathbf{r}}[k] = \frac{1}{\sqrt{N_c}} \sum_{n=0}^{N_c-1} \mathbf{r}[n] e^{-j \frac{2\pi n k}{N_c}}$, $\tilde{\mathbf{w}}[k] = \frac{1}{\sqrt{N_c}} \sum_{n=0}^{N_c-1} \mathbf{w}[n] e^{-j \frac{2\pi n k}{N_c}}$, and $\tilde{\mathbf{H}}[k] = [\tilde{\mathbf{h}}_1[k], \dots, \tilde{\mathbf{h}}_I[k]]$ with $\tilde{\mathbf{h}}_i[k] = \sum_{d=0}^{D-1} \mathbf{h}_i[d] e^{-j \frac{2\pi d k}{N_c}}$. Note that $\tilde{\mathbf{r}}[k] = \tilde{\mathbf{w}}[k]$ for $k = K, \dots, N_c - 1$ as $\tilde{\mathbf{s}}[k] = \mathbf{0}$ in these cases.

B. Quantization Model

We consider that the ADCs at all RF chains are scalar quantizers and have the same resolution (b bits). Define the codebook of a quantizer of b bits as $\mathcal{C} = \{c_0, \dots, c_{N_q-1}\}$, where $N_q = 2^b$ is the number of output levels of the quantizer. The set of quantization thresholds is $\mathcal{T} = \{t_0, \dots, t_{N_q}\}$, where $t_0 = -\infty$ and $t_{N_q} = \infty$ allow inputs with arbitrary power. For standard Gaussian signals, the Lloyd-Max algorithm [19] can find optimal sets \mathcal{C} and \mathcal{T} that achieve the minimum square error (MSE) between the input and output of the quantizer. Let $Q(\cdot)$ denote the quantization function. For a complex signal $x = \Re\{x\} + j\Im\{x\}$, we have $Q(x) = Q(\Re\{x\}) + jQ(\Im\{x\})$ with $Q(\Re\{x\}) = c_{I(\Re\{x\})}$, where $I(\Re\{x\}) = i \in \{0, \dots, N_q - 1\}$ for $\Re\{x\} \in [t_i, t_{i+1}]$, and $Q(\Im\{x\})$ can be obtained in a similar fashion. When the input signal of the quantizer is a vector, $Q(\cdot)$ is applied elementwise.

To model the quantization of the received signal in (2), we first rewrite (2) as

$$\bar{\mathbf{r}} = \bar{\mathbf{H}} \bar{\mathbf{s}} + \bar{\mathbf{w}}, \quad (4)$$

where $\bar{\mathbf{r}} = [\mathbf{r}[N_c - 1]^T, \dots, \mathbf{r}[0]^T]^T$, $\bar{\mathbf{s}} = [\mathbf{s}[N_c - 1]^T, \dots, \mathbf{s}[0]^T]^T$, and $\bar{\mathbf{w}} = [\mathbf{w}[N_c - 1]^T, \dots, \mathbf{w}[0]^T]^T$. Furthermore, $\bar{\mathbf{H}} \in \mathbb{C}^{N_r N_c \times I N_c}$ is a block circulant matrix [15]. Before quantization, the received signal is first combined in the analog domain. Denote the analog combiner as $\mathbf{U}_{\text{RF}} \in \mathbb{C}^{N_r \times N_{\text{RF}}}$, which has constant modulus entries. In the BS, the received time-domain signal $\bar{\mathbf{r}}$ is first combined by \mathbf{U}_{RF} and then fed into the ADCs. Therefore, with $\bar{\mathbf{z}}$ denoting the output of the ADCs, we have

$$\bar{\mathbf{z}} = Q(\bar{\mathbf{U}}_{\text{RF}}^H \bar{\mathbf{r}}), \quad (5)$$

where $\bar{\mathbf{U}}_{\text{RF}} \triangleq \mathbf{I}_{N_c} \otimes \mathbf{U}_{\text{RF}}$ with \otimes being the Kronecker product. Here, \mathbf{I}_{N_c} represents the identity matrix of size $N_c \times N_c$. The Bussgang decomposition allows to model a non-linear input-output relation of a Gaussian signal as a linear transformation [20]. With the Bussgang decomposition, (5) can be expressed as

$$\bar{\mathbf{z}} = \alpha \bar{\mathbf{U}}_{\text{RF}}^H \bar{\mathbf{r}} + \bar{\boldsymbol{\eta}}, \quad (6)$$

where $\bar{\mathbf{z}} = [\mathbf{z}[N_c - 1]^T, \dots, \mathbf{z}[0]^T]^T$ and $\bar{\boldsymbol{\eta}} = [\boldsymbol{\eta}[N_c - 1]^T, \dots, \boldsymbol{\eta}[0]^T]^T$ denotes the non-Gaussian distortion vector that is uncorrelated to $\bar{\mathbf{r}}$. In (6), $\alpha = 1 - \gamma$ represents the Bussgang gain with γ being the inverse signal-to-quantization-distortion ratio (SQR). For a given resolution, γ is constant, which has been tabulated in [19]. Furthermore, (6) is equivalent to

$$\mathbf{z}[n] = \alpha \mathbf{U}_{\text{RF}}^H \mathbf{r}[n] + \boldsymbol{\eta}[n], \quad n = 0, \dots, N_c - 1. \quad (7)$$

By taking the DFT of both sides of (7), we have

$$\begin{aligned}\tilde{\mathbf{z}}[k] &= \alpha \mathbf{U}_{\text{RF}}^{\text{H}} \tilde{\mathbf{r}}[k] + \tilde{\boldsymbol{\eta}}[k] \\ &= \alpha \sqrt{p} \mathbf{U}_{\text{RF}}^{\text{H}} \tilde{\mathbf{H}}[k] \tilde{\mathbf{s}}[k] + \mathbf{e}[k], \quad k = 0, \dots, N_c - 1,\end{aligned}\quad (8)$$

where $\tilde{\mathbf{z}}[k] = \frac{1}{\sqrt{N_c}} \sum_{n=0}^{N_c-1} \mathbf{z}[n] e^{-j \frac{2\pi n k}{N_c}}$ and $\tilde{\boldsymbol{\eta}}[k] = \frac{1}{\sqrt{N_c}} \sum_{n=0}^{N_c-1} \boldsymbol{\eta}[n] e^{-j \frac{2\pi n k}{N_c}}$. Here, $\mathbf{e}[k] \triangleq \alpha \mathbf{U}_{\text{RF}}^{\text{H}} \tilde{\mathbf{w}}[k] + \tilde{\boldsymbol{\eta}}[k]$ consisting of the AWGN and quantization distortion. Note that the latter is non-Gaussian due to $\tilde{\boldsymbol{\eta}}[k]$.

Let $\mathbf{u}_i[k] \in \mathbb{C}^{N_{\text{RF}}}$ denote the baseband combining vector of the i -th UE at subcarrier k and $\mathbf{U}_{\text{BB}}[k] \triangleq [\mathbf{u}_1[k], \dots, \mathbf{u}_I[k]]$. Therefore, the post-combined signal for the i -th UE at subcarrier k is given by

$$\begin{aligned}\hat{x}_i[k] &= \underbrace{\alpha \sqrt{p} \mathbf{u}_i[k]^{\text{H}} \mathbf{U}_{\text{RF}}^{\text{H}} \mathbf{h}_i[k] \tilde{s}_i[k]}_{\text{desired signal}} \\ &+ \underbrace{\alpha \sqrt{p} \sum_{j \neq i} \mathbf{u}_i[k]^{\text{H}} \mathbf{U}_{\text{RF}}^{\text{H}} \mathbf{h}_j[k] \tilde{s}_j[k]}_{\text{interference}} + \underbrace{\mathbf{u}_i[k]^{\text{H}} \mathbf{e}[k]}_{\text{AWGN and quantization distortion}}.\end{aligned}\quad (9)$$

III. HYBRID RECEIVER DESIGN

A. Problem formulation

Based on (9), the signal-to-interference-plus-noise-and-distortion ratio (SINDR) of the i -th UE at subcarrier k can be expressed as

$$\zeta_i[k] = \frac{p \alpha^2 |\mathbf{u}_i[k]^{\text{H}} \mathbf{U}_{\text{RF}}^{\text{H}} \mathbf{h}_i[k]|^2}{p \alpha^2 \sum_{j \neq i} |\mathbf{u}_i[k]^{\text{H}} \mathbf{U}_{\text{RF}}^{\text{H}} \mathbf{h}_j[k]|^2 + \mathbf{u}_i[k]^{\text{H}} \mathbf{C}_{\mathbf{e}_k} \mathbf{u}_i[k]}, \quad (10)$$

where $\mathbf{C}_{\mathbf{e}_k} \triangleq \mathbb{E}[\mathbf{e}[k] \mathbf{e}[k]^{\text{H}}] = \mathbf{C}_{\tilde{\boldsymbol{\eta}}_k} + \alpha^2 \sigma_n^2 \mathbf{U}_{\text{RF}}^{\text{H}} \mathbf{U}_{\text{RF}}$ and $\mathbf{C}_{\tilde{\boldsymbol{\eta}}_k} \triangleq \mathbb{E}[\tilde{\boldsymbol{\eta}}[k] \tilde{\boldsymbol{\eta}}[k]^{\text{H}}]$ denotes the frequency-domain covariance matrix of the quantization distortion. Treating the interference-plus-noise-and-distortion term as a Gaussian random variable with the same variance, we obtain an SE as [21]

$$R = \frac{1}{K} \sum_{k=1}^K \sum_{i=1}^I \log_2(1 + \zeta_i[k]). \quad (11)$$

It is observed that $\mathbf{C}_{\tilde{\boldsymbol{\eta}}_k}$ is required to compute the SE in (11). However, obtaining $\mathbf{C}_{\tilde{\boldsymbol{\eta}}_k}$ is challenging because both the temporal and spatial correlations of the quantization distortion need to be considered. We herein present a closed-form approximation with the following proposition.

Proposition 1 $\mathbf{C}_{\tilde{\boldsymbol{\eta}}_k}$ can be approximated as

$$\begin{aligned}\mathbf{C}_{\tilde{\boldsymbol{\eta}}_k} &\approx \gamma(1 - \gamma) \frac{p}{N_c} \sum_{k=0}^{K-1} \text{diag} \left(\mathbf{U}_{\text{RF}}^{\text{H}} \tilde{\mathbf{H}}[k] \tilde{\mathbf{H}}[k]^{\text{H}} \mathbf{U}_{\text{RF}} \right) \\ &+ \gamma(1 - \gamma) \sigma_n^2 \mathbf{U}_{\text{RF}}^{\text{H}} \mathbf{U}_{\text{RF}},\end{aligned}\quad (12)$$

which becomes more accurate at a lower SNR or at a higher SNR with a low OSR and a high ADC resolution.

Proposition 1 can be obtained through the DFT of the time-domain correlation matrix $\mathbf{C}_{\mathbf{r}}[l] = \mathbb{E}[\mathbf{r}[n] \mathbf{r}[n-l]^{\text{H}}]$ and $\mathbf{C}_{\boldsymbol{\eta}}[l] = \mathbb{E}[\boldsymbol{\eta}[n] \boldsymbol{\eta}[n-l]^{\text{H}}]$ as well as the diagonal approximation $\mathbf{C}_{\boldsymbol{\eta}}[0] \approx \gamma(1 - \gamma) \text{diag}(\mathbf{U}_{\text{RF}}^{\text{H}} \mathbf{C}_{\mathbf{r}}[0] \mathbf{U}_{\text{RF}})$ [22]. The detailed proof is omitted due to limited space. Note that $\mathbf{C}_{\boldsymbol{\eta}}[l]$ includes the temporal and spatial correlations of the quantization distortion.

With (12), we obtain the SINDR as

$$\zeta_i[k] \approx \frac{|\mathbf{u}_i[k]^{\text{H}} \mathbf{U}_{\text{RF}}^{\text{H}} \mathbf{h}_i[k]|^2}{\sum_{j \neq i} |\mathbf{u}_i[k]^{\text{H}} \mathbf{U}_{\text{RF}}^{\text{H}} \mathbf{h}_j[k]|^2 + \mathbf{u}_i[k]^{\text{H}} \mathbf{C}_{\mathbf{e}} \mathbf{u}_i[k]}, \quad (13)$$

where

$$\mathbf{C}_{\mathbf{e}} \triangleq \frac{\gamma}{(1 - \gamma)\beta} \mathbf{H}_{\mathbf{e}} + \frac{1}{\rho(1 - \gamma)} \mathbf{U}_{\text{RF}}^{\text{H}} \mathbf{U}_{\text{RF}}, \quad (14)$$

with $\mathbf{H}_{\mathbf{e}} \triangleq \frac{1}{K} \sum_{k=0}^{K-1} \text{diag} \left(\mathbf{U}_{\text{RF}}^{\text{H}} \tilde{\mathbf{H}}[k] \tilde{\mathbf{H}}[k]^{\text{H}} \mathbf{U}_{\text{RF}} \right)$ and $\rho \triangleq p/\sigma_n^2$ being the SNR. We note that $\mathbf{C}_{\mathbf{e}}$ represents the covariance of the overall effective noise of the system, which is jointly affected by the OSR, the ADC resolution, and the SNR.

With (14) obtained, we aim to jointly optimize the analog and baseband combiner to maximize the SE. Specifically, the problem of interest is formulated as

$$\begin{aligned}&\underset{\mathbf{U}_{\text{RF}}, \{\mathbf{U}_{\text{BB}}[k]\}_{k=1}^K}{\text{maximize}} && R\end{aligned}\quad (15a)$$

$$\text{subject to} \quad |\mathbf{U}_{\text{RF}}(m, n)| = \frac{1}{\sqrt{N_{\text{R}}}}, \quad \forall m, n, \quad (15b)$$

where $\mathbf{U}_{\text{RF}}(m, n)$ denotes the entry of \mathbf{U}_{RF} at the m -th row and the n -th column. Due to the hardware constraint of the analog combiner and the non-convex objective function, solving problem (15) is significantly challenging. In the following, we devise an efficient solution to (15) based on fractional programming [23].

B. Solution

We first show that (15) can be solved with an equivalent but more tractable problem in the following proposition.

Proposition 2 The objective function is equivalent to the maximization of

$$\begin{aligned}f_q(\mathbf{U}_{\text{RF}}, \{\mathbf{U}_{\text{BB}}[k], \mathbf{r}[k], \mathbf{q}[k]\}_{k=1}^K) \\ = \frac{G}{K \ln 2} + \frac{1}{K} \sum_{(k,i)} \log_2(1 + r_i[k]) - \frac{1}{K \ln 2} \sum_{(k,i)} r_i[k]\end{aligned}\quad (16)$$

with respect to $\{\mathbf{r}[k], \mathbf{q}[k]\}_{k=1}^K$, where $\mathbf{r}[k] \in \mathbb{R}^I$, $\forall k$ and $\mathbf{q}[k] \in \mathbb{C}^I$, $\forall k$ are introduced auxiliary variables, and

$$\begin{aligned}G \triangleq \sum_{(k,i)} 2\sqrt{(r_i[k] + 1)} \Re\{q_i[k]^* \mathbf{u}_i[k]^{\text{H}} \mathbf{U}_{\text{RF}}^{\text{H}} \mathbf{h}_i[k]\} \\ - \sum_{(k,i)} |q_i[k]|^2 \left(\sum_{j=1}^I |\mathbf{u}_i[k]^{\text{H}} \mathbf{U}_{\text{RF}}^{\text{H}} \mathbf{h}_j[k]|^2 + \mathbf{u}_i[k]^{\text{H}} \mathbf{C}_{\mathbf{e}} \mathbf{u}_i[k] \right).\end{aligned}\quad (17)$$

Here, $r_i[k]$ and $q_i[k]$ are the i -th elements of $\mathbf{r}[k]$ and $\mathbf{q}[k]$, respectively. The optimal solution to $r_i[k]$ and $q_i[k]$ are given by

$$r_i^*[k] = \frac{|\mathbf{u}_i[k]^{\text{H}} \mathbf{U}_{\text{RF}}^{\text{H}} \mathbf{h}_i[k]|^2}{\sum_{j \neq i} |\mathbf{u}_i[k]^{\text{H}} \mathbf{U}_{\text{RF}}^{\text{H}} \mathbf{h}_j[k]|^2 + \mathbf{u}_i[k]^{\text{H}} \mathbf{C}_{\mathbf{e}} \mathbf{u}_i[k]}, \quad (18)$$

$$q_i^*[k] = \frac{\sqrt{(r_i[k] + 1)} \mathbf{u}_i[k]^{\text{H}} \mathbf{U}_{\text{RF}}^{\text{H}} \mathbf{h}_i[k]}{\sum_{j=1}^I |\mathbf{u}_i[k]^{\text{H}} \mathbf{U}_{\text{RF}}^{\text{H}} \mathbf{h}_j[k]|^2 + \mathbf{u}_i[k]^{\text{H}} \mathbf{C}_{\mathbf{e}} \mathbf{u}_i[k]}.\quad (19)$$

We omit the detailed proof here due to limited space. Proposition 2 shows that the solutions to (15) can be obtained as

$$\begin{aligned} & \{\mathbf{U}_{\text{RF}}^*, \{\mathbf{U}_{\text{BB}}^*[k], \mathbf{r}^*[k], \mathbf{q}^*[k]\}_{k=1}^K\} = \\ & \arg \max_{\mathbf{U}_{\text{RF}}, \{\mathbf{U}_{\text{BB}}[k], \mathbf{r}[k], \mathbf{q}[k]\}_{k=1}^K} f_q(\mathbf{U}_{\text{RF}}, \{\mathbf{U}_{\text{BB}}[k], \mathbf{r}[k], \mathbf{q}[k]\}_{k=1}^K) \\ & \text{subject to (15b)}. \end{aligned} \quad (20)$$

Let $\{\mathbf{U}_{\text{BB}}[k]\}$, $\{\mathbf{r}[k]\}$ and $\{\mathbf{q}[k]\}$ represent $\{\mathbf{U}_{\text{BB}}[k]\}_{k=1}^K$, $\{\mathbf{r}[k]\}_{k=1}^K$ and $\{\mathbf{q}[k]\}_{k=1}^K$ for short. It is observed that we can iteratively update \mathbf{U}_{RF} , $\{\mathbf{U}_{\text{BB}}[k]\}$, $\{\mathbf{r}[k]\}$ and $\{\mathbf{q}[k]\}$ to solve problem (20). Since the optimal $\{\mathbf{r}^*[k]\}$ and $\{\mathbf{q}^*[k]\}$ are given in (18) and (19), respectively, we aim to develop the solution to \mathbf{U}_{RF} and $\{\mathbf{U}_{\text{BB}}[k]\}$ next.

1) *Analog Combiner Design:* Define $\underline{\mathbf{H}} \triangleq \frac{1}{K} \sum_{k=0}^{K-1} \tilde{\mathbf{H}}[k] \tilde{\mathbf{H}}[k]^H$, $\mathbf{Y}[k] \triangleq \sum_{i=1}^I \mathbf{h}_i[k] \mathbf{h}_i^H[k]$, $\forall k$, and

$$\mathbf{X} \triangleq \sum_{(k,i)} \sqrt{(r_i[k] + 1)} q_i[k]^* \mathbf{h}_i[k] \mathbf{u}_i[k]^H, \quad (21)$$

$$\mathbf{Z}[k] \triangleq \sum_{i=1}^I |q_i[k]|^2 \mathbf{u}_i[k] \mathbf{u}_i^H[k], \quad \forall k. \quad (22)$$

The objective function with respect to \mathbf{U}_{RF} can be expressed as

$$\begin{aligned} g(\mathbf{U}_{\text{RF}}) & \triangleq 2\Re\{\text{Tr}(\mathbf{X}\mathbf{U}_{\text{RF}}^H)\} - \sum_{k=1}^K \text{Tr}(\mathbf{Z}[k]\mathbf{U}_{\text{RF}}^H\mathbf{Y}[k]\mathbf{U}_{\text{RF}}) \\ & - \frac{\gamma}{(1-\gamma)\beta} \sum_{k=1}^K \text{Tr}(\text{diag}(\mathbf{Z}[k])\mathbf{U}_{\text{RF}}^H\underline{\mathbf{H}}\mathbf{U}_{\text{RF}}) \\ & - \frac{1}{\rho(1-\gamma)} \sum_{k=1}^K \text{Tr}(\mathbf{Z}[k]\mathbf{U}_{\text{RF}}^H\mathbf{U}_{\text{RF}}). \end{aligned} \quad (23)$$

With other variables fixed, the design of the analog combiner \mathbf{U}_{RF} can be expressed as

$$\mathbf{U}_{\text{RF}}^* = \arg \max_{\mathbf{U}_{\text{RF}}} g(\mathbf{U}_{\text{RF}}) \quad \text{subject to (15b)}. \quad (24)$$

We employ the project gradient ascend (PGA) method [24] to efficiently solve \mathbf{U}_{RF}^* iteratively. The gradient of $g(\mathbf{U}_{\text{RF}})$ is given as

$$\begin{aligned} \nabla_{\mathbf{U}_{\text{RF}}} g(\mathbf{U}_{\text{RF}}) & = 2\mathbf{X} - \frac{2}{\rho(1-\gamma)} \sum_{k=1}^K \mathbf{U}_{\text{RF}} \mathbf{Z}[k] \\ & - \frac{2\gamma}{(1-\gamma)\beta} \sum_{k=1}^K \underline{\mathbf{H}} \mathbf{U}_{\text{RF}} \text{diag}(\mathbf{Z}[k]) - 2 \sum_{k=1}^K \mathbf{Y}[k] \mathbf{U}_{\text{RF}} \mathbf{Z}[k]. \end{aligned} \quad (25)$$

The detailed procedure is summarized in Algorithm 1. In step 4, the normalized gradient $\nabla \mathbf{U}_{\text{RF}}$ is obtained and employed later in step 6, where the step size μ is determined by the backtracking line search method as in step 5, and $[\cdot]_{\mathcal{U}}$ denotes the projection into \mathcal{U} , defined as $\mathcal{U} \triangleq \{\mathbf{U}_{\text{RF}} : |\mathbf{U}_{\text{RF}}(m, n)| = \frac{1}{\sqrt{N_r}}, \forall m, n\}$. The iterations continue until the procedure satisfies the stopping criteria.

2) *Digital Combiner Design:* For given \mathbf{U}_{RF} and $\{\mathbf{r}[k], \mathbf{q}[k]\}_{k=1}^K$, the design of the digital combiner is formulated as

$$\{\mathbf{U}_{\text{BB}}^*[k]\}_{k=1}^K = \arg \max G, \quad (26)$$

Algorithm 1: PGA algorithm for problem (24)

Output: \mathbf{U}_{RF}
1 Initialize $\iota \in (0, 0.5)$, $c \in (0, 1)$, $\mathbf{U}_{\text{RF}} \in \mathcal{U}$, and ϵ ;
2 **repeat**
3 Set $\mathbf{U}'_{\text{RF}} \leftarrow \mathbf{U}_{\text{RF}}$.
4 Obtain $\nabla \mathbf{U}_{\text{RF}} = \frac{\nabla_{\mathbf{U}_{\text{RF}}} g(\mathbf{U}_{\text{RF}})}{\|\nabla_{\mathbf{U}_{\text{RF}}} g(\mathbf{U}_{\text{RF}})\|_F}$ with (25).
5 Start with $\mu = 1$, **repeat** $\mu \leftarrow c\mu$ until
 $g([\mathbf{U}_{\text{RF}} + \mu \nabla \mathbf{U}_{\text{RF}}]_{\mathcal{U}}) > g(\mathbf{U}_{\text{RF}}) + \iota \mu \|\nabla \mathbf{U}_{\text{RF}}\|_F^2$.
6 Update \mathbf{U}_{RF} as $\mathbf{U}_{\text{RF}} \leftarrow [\mathbf{U}_{\text{RF}} + \mu \nabla \mathbf{U}_{\text{RF}}]_{\mathcal{U}}$.
7 **until** $|g(\mathbf{U}'_{\text{RF}}) - g(\mathbf{U}_{\text{RF}})| \leq \epsilon$;

Algorithm 2: Hybrid Combiner Design for Problem (15)

Output: \mathbf{U}_{RF}^* , $\{\mathbf{U}_{\text{BB}}[k]^*\}_{k=1}^K$
1 Initialize $\mathbf{U}_{\text{RF}} \in \mathcal{U}$ and $\{\mathbf{U}_{\text{BB}}[k]\}_{k=1}^K$.
2 **repeat**
3 Update $\{\mathbf{r}[k]^*\}_{k=1}^K$ by (18).
4 Update $\{\mathbf{q}[k]^*\}_{k=1}^K$ by (19).
5 Update \mathbf{U}_{RF} by Algorithm 1.
6 Update $\{\mathbf{U}_{\text{BB}}[k]^*\}_{k=1}^K$ by (27).
7 **until** stopping criteria is satisfied;

where G is given in (17). With the first-order condition of optimality, we can derive the optimal digital combiner of subcarrier k for user i as

$$\mathbf{u}_i^*[k] = \xi_i[k] (\mathbf{U}_{\text{RF}}^H \mathbf{Y}[k] \mathbf{U}_{\text{RF}} + \mathbf{C}_e)^{-1} \mathbf{U}_{\text{RF}}^H \mathbf{h}_i[k], \quad \forall i, k, \quad (27)$$

where $\xi_i[k] \triangleq \frac{q_i[k]^* \sqrt{r_i[k] + 1}}{|q_i[k]|^2}$.

The overall proposed algorithm for solving problem (15) is summarized in Algorithm 2, which can be initialized as follows. Let the singular-value decomposition (SVD) of $\underline{\mathbf{H}}$ be $\underline{\mathbf{H}} = \mathbf{V} \mathbf{\Sigma} \mathbf{V}^H$, where $\mathbf{V} = [\mathbf{v}_1, \dots, \mathbf{v}_{N_r}]$ is a unitary matrix, and $\mathbf{\Sigma}$ is a diagonal matrix with singular values on the main diagonal in descending order. Then, \mathbf{U}_{RF} can be initialized as

$$\mathbf{U}_{\text{RF}} = \frac{1}{\sqrt{M}} e^{j\angle \hat{\mathbf{V}}}, \quad (28)$$

where $\hat{\mathbf{V}} = [\mathbf{v}_1, \dots, \mathbf{v}_{N_{\text{RF}}}]$, and $\angle \hat{\mathbf{V}}$ denotes the phase of the entries of $\hat{\mathbf{V}}$. The baseband combiner can be initialized based on the minimum mean square error (MMSE) criterion. Specifically, we have

$$\mathbf{u}_i[k] = \alpha \sqrt{p} \mathbf{J}[k]^{-1} \mathbf{U}_{\text{RF}}^H \mathbf{h}_i[k], \quad \forall i, k, \quad (29)$$

where $\mathbf{J}[k] \triangleq \alpha^2 p \left(\sum_{i=1}^I \mathbf{U}_{\text{RF}}^H \mathbf{h}_i[k] \mathbf{h}_i^H[k] \mathbf{U}_{\text{RF}} + \mathbf{C}_e \right)$. We note that Algorithm 2 converges to at least a stationary point since the objective function (16) is monotonically nondecreasing over iterations [23]. With $I \leq N_{\text{RF}}$ and $N_{\text{RF}} \ll N_r$, the complexity of Algorithm 1 and Algorithm 2 are approximately $\mathcal{O}(4N_{\text{pga}} K N_r^2 N_{\text{RF}})$ and $N_{\text{iter}} \mathcal{O}(4N_{\text{pga}} K N_r^2 N_{\text{RF}} + 2K N_r^2 N_{\text{RF}}^2)$, respectively, which are caused mainly by matrix multiplication. Here, N_{pga} and N_{iter} denote the number of iterations of Algorithm 1 and Algorithm 2, respectively.

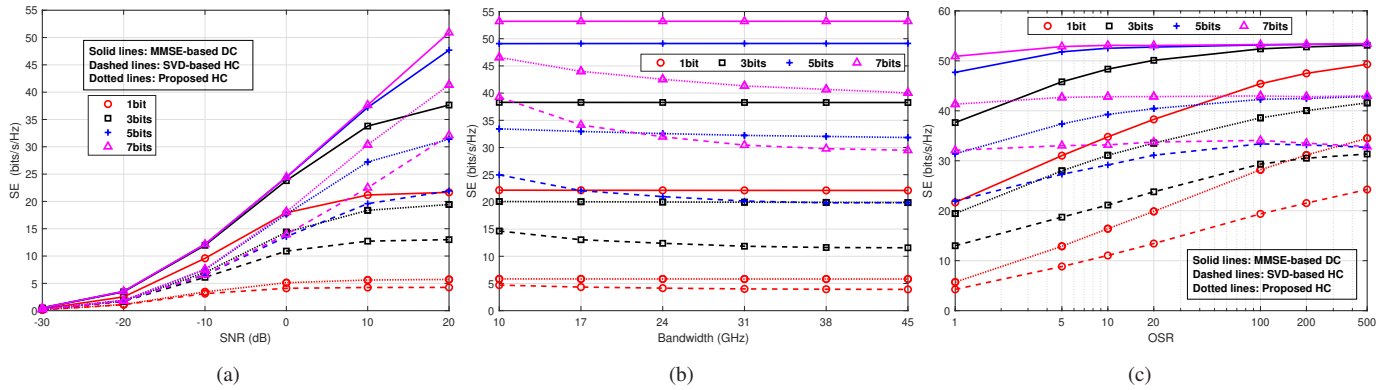


Fig. 1. SE versus SNR, bandwidth, and OSR with $N_r = 128$ and $N_{RF} = I = 4$. Fig. (a): SE versus SNR (ρ) with $\beta = 1$ and $B_w = 12.8$ GHz. Fig. (b): SE versus bandwidth (B_w) with $\beta = 1$ and SNR = 20 dB. Fig. (c): SE versus OSR (β) with SNR = 20 dB and $B_w = 12.8$ GHz. Among the three figures, the groups of solid, dashed, and dotted lines represent the MMSE-based DC, SVD-based HC, and the proposed HC schemes, respectively.

IV. SIMULATION RESULTS

In this section, we show numerical results to demonstrate the proposed algorithms. In the simulations, the channel vector between the i -th UE and the BS at subcarrier k is modeled as [18]

$$\mathbf{h}_i[k] = \sqrt{\frac{N_r}{L}} \sum_{\ell=1}^L g_{i,\ell}[k] \mathbf{a}(\theta_{i,\ell}, f_k), \quad (30)$$

where $g_{i,\ell}[k] \triangleq \sum_{d=0}^{D-1} \lambda_{i,\ell} p(dT_s - \tau_{i,\ell}) e^{-j\frac{2\pi k}{N_c} d}$, with $\lambda_{i,\ell}$, $\tau_{i,\ell}$, and $\theta_{i,\ell}$ being the ℓ -th path gain, path delay and angle-of-arrival, respectively. In the simulations, the pulse-shaping filter $p(t)$ is modeled by the raised cosine function with the roll-off factor being 1. We assume $L = 3$, $\lambda_{i,\ell} \sim \mathcal{CN}(0, 1)$, $\tau_{i,\ell} \sim \mathcal{U}[0, \frac{D_0}{B_w}]$ with $D_0 = K/4$ as in [16], and $\theta_{i,\ell} \sim \mathcal{U}[0, 2\pi]$. Here, $\mathcal{U}[a, b]$ represents the uniform distribution in the interval $[a, b]$. The array steering vector is expressed as $\mathbf{a}(\theta, f) = \frac{1}{\sqrt{N_r}} [1, e^{-j\pi \frac{f}{f_c} \sin(\theta)}, \dots, e^{-j(N_r-1)\pi \frac{f}{f_c} \sin(\theta)}]$. Furthermore, we set $f_c = 300$ GHz and $K = 128$. The following results are obtained by averaging over 10^3 independent channel realizations.

Fig. 1 shows the SE performance versus the SNR, the bandwidth, and the OSR with $N_r = 128$ and $N_{RF} = I = 4$, wherein the MMSE-based DC denotes the digital MMSE combiner, and the SVD-based HC represents the hybrid combiner design with (28) and (29), which has been studied in [25]. It is observed from Fig. 1(a) that the proposed HC design significantly outperforms the SVD-based scheme, especially at high SNRs. For instance, with 3-bit quantization, the former improves the SE of the latter by 43% at SNR = 20 dB. However, the HC schemes exhibit large SE gaps compared to the MMSE-based DC, especially for low-resolution cases. With 7-bit quantization, the proposed HC attains 80% of the SE achieved by the MMSE-based DC. In contrast, the former only achieves 26% SE of the latter with 1-bit quantization. Additionally, we observe from Fig. 1(b) that the SE performance of the HC schemes degrades with increasing bandwidth due to the beam squint effect, aligned with the observations in [17], [18], [24]. Notably, the achievable SE of the proposed HC is less affected by the increase in bandwidth for lower

resolution systems. For example, when bandwidth increases from 10 GHz to 45 GHz, the achievable SE of the proposed scheme with 7-bit quantization decreases by 6.5 bit/s/Hz, whereas it is 1.6 bit/s/Hz with 5-bit quantization. This is likely because the quantization distortion overwhelms the array gain loss due to squinted beams in low-resolution systems.

Fig. 1(c) shows the SE versus the OSR with SNR = 20 dB and $B_w = 12.8$ GHz. It is shown that increasing the OSR can significantly enhance the achievable SE of both digital and hybrid receivers, especially with low-resolution ADCs. For instance, with 1-bit quantization, a 126% SE improvement is achieved when the OSR increases from 1 to 5, whereas it is 44% with 3-bit quantization. Such results align with the findings in [16]. When the OSR is sufficiently large, the quantization distortion can be fully suppressed (as seen from (14)), leading to similar SE of the 3–7 bit DC or HC schemes at $\beta = 500$. However, increasing the OSR also results in a higher power consumption for ADCs. This is because a b -bit ADC typically has a power consumption of $P_{ADC} = \kappa f_s 2^b$ [16] where κ and f_s represent the figure of merit (FoM) and the sampling frequency, respectively. Therefore, the OSR requires to be judiciously chosen to achieve a satisfactory tradeoff between SE and EE. Next, we evaluate the achievable EE.

The EE is defined as the ratio between the SE and the total power consumption of the receiver [9]. The total power consumption of the fully digital receiver and the considered hybrid receiver are given as $P_D = N_r (P_{LNA} + P_{RF} + 2P_{ADC})$ and $P_H = N_r (P_{LNA} + P_{SP} + N_{RF} P_{PS}) + N_{RF} (P_{RF} + P_C + 2P_{ADC})$ where P_{LNA} , P_{RF} , P_{ADC} , P_{SP} , P_C , and P_{PS} represent the power consumption of a low-noise amplifier (LNA), an RF chain, an ADC, a splitter, a combiner and a phase shifter (PS), respectively. In the following simulations, we set $P_{RF} = 43$ mW, $P_{LNA} = 25$ mW, $P_{SP}/P_C = 19.5$ mW, $P_{PS} = 23$ mW, and $\kappa = 494$ fJ/step/Hz [9] for evaluation.

Fig. 2 shows the EE performance of the DC based on MMSE and the proposed HC versus the ADC bits and the OSR with $N_r = 128$, $N_{RF} = I = 4$, SNR = 20 dB, and $B_w = 12.8$ GHz. We make the following observations. First, it is seen that the EE of the digital receiver decreases

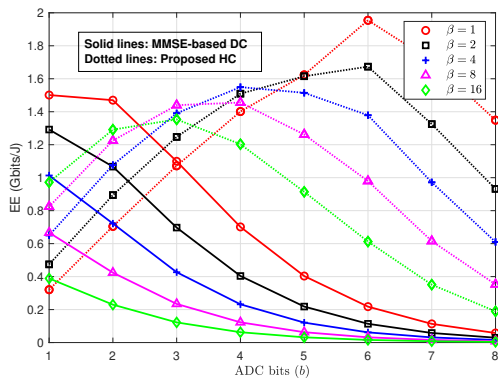


Fig. 2. EE versus ADC bits and OSR with $N_R = 128$, $N_{RF} = I = 4$, SNR = 20 dB, and $B_w = 12.8$ GHz.

with increasing ADC bits and OSR, while that of the hybrid receiver achieves the highest EE at $b \in \{3, 4, 6\}$ for $\beta \in \{1, 2, 4, 8, 16\}$. This is because the large number of RF chains in the digital receiver costs excessively high power consumption, which offsets the resultant SE improvements due to more bits and higher OSR and leads to lower EE. In contrast, the number of RF chains in the hybrid receiver is significantly less than that of the digital one, making the increase of ADC bits beneficial to EE enhancements when ADC bits are relatively smaller. Second, we can observe that increasing the OSR for $b \in \{1, 2\}$ in the hybrid receiver can significantly improve the EE while that for $b \geq 5$ causes a reduced EE. This is because increasing the OSR for higher resolution ADCs contributes only to minor SE improvements but results in significantly higher power consumption for ADCs. Third, from the EE maximization perspective, using digital receiver with 1–2 bit quantization without oversampling can achieve better performance than the hybrid receiver. In contrast, the hybrid one with more than 3-bit quantization and oversampling performs significantly better than the digital receiver.

V. CONCLUSION

We studied the hybrid receiver design in a massive MIMO-OFDM system with low-resolution ADCs and oversampling. Specifically, we first derived a closed-form approximation for the frequency-domain covariance matrix of the quantization distortion, which facilitates the evaluation of SE. Then we proposed an efficient algorithm to jointly optimize the analog and digital combiner to maximize the SE. Numerical simulations validate the superiority of the proposed algorithm over the benchmarks considered. Furthermore, the results show that the hybrid receiver is less affected by the beam squint effect in a low-resolution system. In addition, the EE comparison shows that the proposed hybrid receiver design with oversampling significantly outperforms the considered digital receiver for slightly higher (larger than 3) ADC bits.

REFERENCES

- [1] N. Rajatheva, I. Atzeni, E. Björnson *et al.*, “White paper on broadband connectivity in 6G,” <https://oulurepo.oulu.fi/handle/10024/36799>, 2020.
- [2] M. A. Albreem, M. Juntti, and S. Shahabuddin, “Massive MIMO detection techniques: A survey,” *IEEE Commun. Surveys Tuts.*, vol. 21, no. 4, pp. 3109–3132, 2019.

- [3] E. Björnson, L. Van der Perre, S. Buzzi, and E. G. Larsson, “Massive MIMO in sub-6 GHz and mmWave: Physical, practical, and use-case differences,” *IEEE Wireless Commun.*, vol. 26, no. 2, pp. 100–108, 2019.
- [4] A. Shafie, N. Yang, C. Han, J. M. Jornet, M. Juntti, and T. Kürner, “Terahertz communications for 6g and beyond wireless networks: Challenges, key advancements, and opportunities,” *IEEE Netw.*, vol. 37, no. 3, pp. 162–169, 2022.
- [5] B. Murmann, “The race for the extra decibel: A brief review of current ADC performance trajectories,” *IEEE Solid-State Circuits Mag.*, vol. 7, no. 3, pp. 58–66, 2015.
- [6] Y. Li, C. Tao, G. Seco-Granados, A. Mezghani, A. L. Swindlehurst, and L. Liu, “Channel estimation and performance analysis of one-bit massive MIMO systems,” *IEEE Trans. Signal Process.*, vol. 65, no. 15, pp. 4075–4089, 2017.
- [7] M. Ma, N. T. Nguyen, and M. Juntti, “Closed-form hybrid beamforming solution for spectral efficiency upper bound maximization in mmWave MIMO-OFDM systems,” in *Proc. IEEE Veh. Technol. Conf.*, 2021.
- [8] I. Atzeni and A. Tölö, “Channel estimation and data detection analysis of massive MIMO with 1-bit ADCs,” *IEEE Trans. Wireless Commun.*, vol. 21, no. 6, pp. 3850–3867, 2022.
- [9] W. B. Abbas, F. Gomez-Cuba, and M. Zorzi, “Millimeter wave receiver efficiency: A comprehensive comparison of beamforming schemes with low resolution ADCs,” *IEEE Trans. Wireless Commun.*, vol. 16, no. 12, pp. 8131–8146, 2017.
- [10] J. Mo, A. Alkhateeb, S. Abu-Surra, and R. W. Heath, “Hybrid architectures with few-bit ADC receivers: Achievable rates and energy-rate tradeoffs,” *IEEE Trans. Commun.*, vol. 16, no. 4, pp. 2274–2287, 2017.
- [11] K. Roth, H. Pirzadeh, A. L. Swindlehurst, and J. A. Nossek, “A comparison of hybrid beamforming and digital beamforming with low-resolution ADCs for multiple users and imperfect CSI,” *IEEE J. Sel. Topics Signal Process.*, vol. 12, no. 3, pp. 484–498, 2018.
- [12] S. Jacobsson, G. Durisi, M. Coldrey, and C. Studer, “Linear precoding with low-resolution DACs for massive MU-MIMO-OFDM downlink,” *IEEE Trans. Wireless Commun.*, vol. 18, no. 3, pp. 1595–1609, 2019.
- [13] C. Mollen, J. Choi, E. G. Larsson, and R. W. Heath, “Uplink performance of wideband massive MIMO with one-bit ADCs,” *IEEE Trans. Wireless Commun.*, vol. 16, no. 1, pp. 87–100, 2016.
- [14] C. Studer and G. Durisi, “Quantized massive MU-MIMO-OFDM uplink,” *IEEE Trans. Commun.*, vol. 64, no. 6, pp. 2387–2399, 2016.
- [15] A. B. Üçüncü, E. Björnson, H. Johansson, A. Ö. Yılmaz, and E. G. Larsson, “Performance analysis of quantized uplink massive MIMO-OFDM with oversampling under adjacent channel interference,” *IEEE Trans. Commun.*, vol. 68, no. 2, pp. 871–886, 2019.
- [16] M. Ma, N. T. Nguyen, I. Atzeni, and M. Juntti, “Analysis of oversampling in uplink massive MIMO-OFDM with low-resolution ADCs,” in *Proc. Int. Workshop Signal Process. Adv. in Wireless Commun.*, 2023.
- [17] L. Dai, J. Tan, Z. Chen, and H. V. Poor, “Delay-phase precoding for wideband THz massive MIMO,” *IEEE Trans. Wireless Commun.*, vol. 21, no. 9, pp. 7271–7286, 2022.
- [18] M. Ma, N. T. Nguyen, and M. Juntti, “Beam squint analysis and mitigation via hybrid beamforming design in THz communications,” in *Proc. IEEE Int. Conf. Commun.*, 2023.
- [19] J. Max, “Quantizing for minimum distortion,” *IRE Trans. Inf. Theory*, vol. 6, no. 1, pp. 7–12, 1960.
- [20] J. J. Bussgang, “Crosscorrelation functions of amplitude-distorted Gaussian signals,” Res. Lab. Electron., Massachusetts Inst. Technol., Tech. Rep., 1952.
- [21] L. Fan, S. Jin, C.-K. Wen, and H. Zhang, “Uplink achievable rate for massive MIMO systems with low-resolution ADC,” *IEEE Commun. Lett.*, vol. 19, no. 12, pp. 2186–2189, 2015.
- [22] A. Mezghani and J. A. Nossek, “Capacity lower bound of MIMO channels with output quantization and correlated noise,” in *Proc. IEEE Int. Symp. Inf. Theory*, 2012.
- [23] K. Shen and W. Yu, “Fractional programming for communication systems—part I: Power control and beamforming,” *IEEE Trans. Signal Process.*, vol. 66, no. 10, pp. 2616–2630, 2018.
- [24] M. Ma, N. T. Nguyen, and M. Juntti, “Switch-based hybrid beamforming transceiver design for wideband communications with beam squint,” *arXiv preprint arXiv:2210.06890*, 2022.
- [25] Y. Zhu and T. Yang, “Low complexity hybrid beamforming for uplink multiuser mmwave MIMO systems,” in *Proc. IEEE Wireless Commun. and Networking Conf.*, 2017.